

# Super-enhanced Sensitivity in Non-Hermitian Systems at Infernal Points

Shu-Xuan Wang<sup>1,\*</sup> and Zhongbo Yan<sup>1,†</sup>

<sup>1</sup>*Guangdong Provincial Key Laboratory of Magnetoelectric Physics and Devices,  
State Key Laboratory of Optoelectronic Materials and Technologies,  
School of Physics, Sun Yat-sen University, Guangzhou 510275, China*

(Dated: May 21, 2025)

The emergence of exceptional points in non-Hermitian systems represents an intriguing phenomenon characterized by the coalescence of eigenenergies and eigenstates. When a system approaches an exceptional point, it exhibits a heightened sensitivity to perturbations compared to the conventional band degeneracy observed in Hermitian systems. This sensitivity, manifested in the splitting of the eigenenergies, is amplified as the order of the exceptional point increases. Infernal points constitute a unique subclass of exceptional points, distinguished by their order escalating with the expansion of the system's size. In this paper, we show that, when a non-Hermitian system is at an infernal point, a perturbation of strength  $\epsilon$ , which couples the two opposing boundaries of the system, causes the eigenenergies to split according to the law  $\sqrt[k]{\epsilon}$ , where  $k$  is an integer proportional to the system's size. Utilizing the perturbation theory of Jordan matrices, we demonstrate that the exceptional sensitivity of the eigenenergies at infernal points to boundary-coupling perturbations is a ubiquitous phenomenon, irrespective of the specific form of the non-Hermitian Hamiltonians. Notably, we find that this phenomenon remains robust even when the system deviates substantially from the infernal point. The universal nature and robustness of this phenomenon suggest potential applications in enhancing sensor sensitivity.

*Introduction*—The hermiticity of Hamiltonians is a fundamental assumption in quantum mechanics, yet it has been shown that non-Hermitian Hamiltonians can offer an effective description to many open systems [1, 2]. In recent years, a wide array of exotic phenomena stemming from non-hermiticity have been successively unveiled, sparking increased interest in the study of non-Hermitian physics. Among the myriad of phenomena observed, the emergence of exceptional points (EPs) [3, 4], which signify the coalescence of eigenenergies and eigenstates of the non-Hermitian Hamiltonians, has garnered immense attention due to its potential applications across various fields [5–35]. A particularly intriguing property of EPs is their response to perturbations. Specifically, for a  $k$ -th order EP, where  $k$  represents the number of eigenenergies and eigenstates that coalesce into one, it has been demonstrated that, under the influence of a perturbation with a strength proportional to  $\epsilon$ , the splitting of eigenenergies can be proportional to  $\sqrt[k]{\epsilon}$ . In contrast to the splitting of band degeneracy in Hermitian systems, which scales directly with  $\epsilon$ , it is evident that high-order EPs, in particular, exhibit a much greater sensitivity to infinitesimally small perturbations. This fascinating property is believed to offer significant potential for enhancing sensor sensitivity, prompting a range of theoretical and experimental investigations [36–46].

Recently, a unique subclass of EPs, referred to as infernal points (IPs), has been uncovered in non-Hermitian lattice systems subject to open boundary conditions (OBC) through the framework of non-Bloch band theory [47–50]. At an IP, all eigenstates of the entire system

coalesce into a limited number of eigenstates [50]. In essence, an IP represents a high-order EP, with its order directly proportional to the number of lattice sites. This characteristic is particularly intriguing because it suggests that the order of this class of EPs can be readily incremented by adjusting the system's size, in stark contrast to the conventional method of achieving higher-order EPs, which demands precise parameter tuning under stringent symmetry requirements [51, 52]. As the order is macroscopically large, it is natural to anticipate that an IP will response to a minor perturbation in an exceptionally sensitive manner. However, it is crucial to recognize that not all types of perturbations will result in the same order of splitting, especially for higher-order EPs. Therefore, gaining a general understanding of the conditions required for a perturbation to induce the most pronounced splitting of IPs is of fundamental importance for their in-depth exploration and potential future applications.

In this work, we first employ the one-dimensional (1D) Hatano-Nelson (HN) model to show that boundary-coupling perturbations induce maximal spectral splitting when the system is at an IP. Since non-Hermitian Hamiltonians at IPs inherently adopt a Jordan block structure, we derive general conditions under which perturbations cause the most significant splitting, leveraging Jordan matrix perturbation theory. This framework directly explains the extreme sensitivity of non-Hermitian systems at IPs to boundary-coupling perturbations. Remarkably, we find that this high sensitivity persists even when the system deviates substantially from the IP. This discovery significantly reduces the challenging for the experimental implementation and practical applications of the predicted phenomenon.

*Insights from the HN model*—We begin with the 1D

\* wangshx65@mail.sysu.edu.cn

† yanzhb5@mail.sysu.edu.cn

non-Hermitian HN model [53], which, under OBC, is expressed as follows:

$$H_{HN} = \sum_{n=1}^{L-1} t_r c_{n+1}^\dagger c_n + t_l c_n^\dagger c_{n+1}, \quad (1)$$

where  $t_r$  and  $t_l$  represent the hopping amplitudes, and  $L$  denotes the total number of lattice sites, as depicted in Fig. 1(a). In our previous work [50], we demonstrated that an IP emerges when either  $t_r = 0$  or  $t_l = 0$ , indicating unidirectional hopping. Specifically, when  $t_r = 0$ , the HN Hamiltonian adopts a Jordan block structure, and all eigenstates of the system converge to a single eigenstate of the form  $\Phi_0 = (1, 0, 0, \dots, 0)^T$ , accompanied by the convergence of all eigenenergies to a single energy level at  $E = 0$ .

When the system is at this IP, how do the eigenenergies respond to a perturbation? We find that the impact of the perturbation on the eigenenergies depends on its specific form. For an on-site perturbation of the form  $H' = \epsilon c_n^\dagger c_n$  with  $\epsilon \ll t_l$ , we find the following: (1) When  $n = 1$ , the system retains its single eigenstate  $\Phi_0 = (1, 0, 0, \dots, 0)^T$ , and the sole eigenenergy is shifted to  $E = \epsilon$ . (2) When  $n \in [2, L]$ , there are two eigenenergies: one at  $E = 0$  and the other at  $E = \epsilon$ . The corresponding eigenstates are  $\Phi_0 = (1, 0, 0, \dots, 0)^T$  and  $\Phi_\epsilon = (1, \epsilon/t_l, \dots, (\epsilon/t_l)^{n-1}, 0, \dots, 0)^T$ , respectively. Apparently, the on-site potential perturbation cannot result in the order of splitting desired.

The HN model is renowned for exhibiting non-Hermitian skin effect [54], which notably results in a significant disparity between the energy spectrum observed under periodic boundary conditions (PBC) and that observed under OBC. Having observed this fact, we introduce a perturbation that connects the left and right ends of the chain, as depicted in Fig. 1(a). Specifically, the perturbation takes the form:

$$H_p = \epsilon_r c_1^\dagger c_L + \epsilon_l c_L^\dagger c_1, \quad (2)$$

where  $\epsilon_r$  and  $\epsilon_l$  represent the hopping strength between the two ends of the chain. Accordingly, the matrix form of the Hamiltonian describing the perturbed system at  $t_r = 0$  reads

$$H = \begin{pmatrix} 0 & t_l & & \epsilon_r \\ 0 & 0 & t_l & \\ & \ddots & \ddots & \ddots \\ & & 0 & 0 & t_l \\ \epsilon_l & & & 0 & 0 \end{pmatrix}_{L \times L}. \quad (3)$$

The characteristic polynomial of  $H$  is (see details in Sec. I of the Supplemental Material (SM) [55]),

$$f(\lambda) = \det[H - \lambda \mathbb{I}_{L \times L}] = (-\lambda)^L + (-1)^{L-1} \epsilon_l t_l^{L-1} - \epsilon_r \epsilon_l (-\lambda)^{L-2}. \quad (4)$$

It is readily apparent that  $\epsilon_r$  and  $\epsilon_l$  have remarkably different effects on the eigenenergies. First, consider the

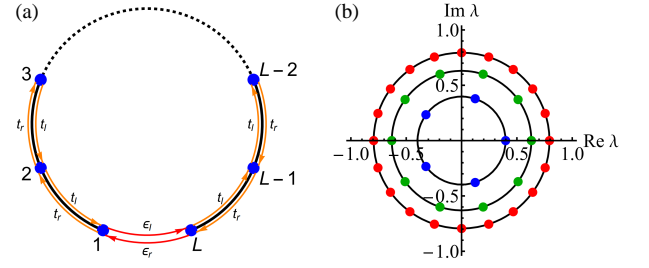


FIG. 1. (a) A schematic diagram of the HN model under a boundary-coupling perturbation.  $\epsilon_r$  and  $\epsilon_l$  characterize the strength of the perturbation. (b) The blue, green and red dots depict eigenenergies for  $L = 5, 10$  and  $20$ , respectively. From the innermost to the outermost, the radius of each circle corresponds to  $\sqrt[5]{10^{-2}}$ ,  $\sqrt[10]{10^{-2}}$  and  $\sqrt[20]{10^{-2}}$ , respectively. The parameters used in (b) are  $t_l = 1$ ,  $t_r = 0$ , and  $\epsilon_r = \epsilon_l = 10^{-2}$ .

scenario where  $\epsilon_l = 0$  but  $\epsilon_r \neq 0$ . Solving  $f(\lambda) = 0$  in this case immediately yields  $\lambda = 0$ , indicating that all eigenenergies remain degenerate. Conversely, if  $\epsilon_r = 0$  but  $\epsilon_l \neq 0$ , then one can find  $L$  roots that satisfy  $f(\lambda) = 0$ . These roots can be compactly expressed as

$$\lambda_p = \left(\frac{\epsilon_l}{t_l}\right)^{\frac{1}{L}} t_l e^{i \frac{2\pi p}{L}}, \quad p = 1, 2, \dots, L. \quad (5)$$

Intriguingly, these  $L$  roots are evenly distributed along the circumference of a circle [56], with the radius of this circle representing the extent of the splitting of the IP. Given that the radius is equal to  $t_l \sqrt[L]{\epsilon_l/t_l}$ , it becomes evident that the eigenenergy splitting is directly proportional to  $\sqrt[L]{\epsilon_l}$ . This signifies that the splitting, which is induced by the perturbation  $\epsilon_l$ , amplifies with the growth of the system's size. However, it is important to note that the splitting does not diverge, rather, it saturates at  $t_l$  in the limit of large  $L$ . This result admits a physical interpretation: in the infinite system size limit, an infinitesimal coupling that slightly modifies the OBC to approach PBC will restore the eigenenergies predicted by Bloch band theory. Indeed, consider the scenario where  $\epsilon_l = t_l$ , which corresponds to the system adopting PBC. In this case, Bloch band theory predicts that all eigenenergies will have the exact form given in Eq. (5).

We have demonstrated above that  $\epsilon_r$  does not influence the IP when  $\epsilon_l$  is equal to zero. When both  $\epsilon_l$  and  $\epsilon_r$  are nonzero but much smaller than  $t_l$ , the splitting should be primarily caused by  $\epsilon_l$ . To illustrate this, Fig. 1(b) displays the eigenenergy distributions obtained by numerically diagonalizing the Hamiltonian given in Eq. (3) under the condition  $\epsilon_r = \epsilon_l = \epsilon$ . The numerical results align well with the analytical solutions presented in Eq. (5), confirming that  $\epsilon_l$  plays the dominant role in inducing the splitting.

*The generality of the phenomenon*—We have demonstrated through the HN model that the eigenenergies at an IP exhibit exceptional sensitivity to boundary-coupling perturbations. This naturally leads to the question: Is this phenomenon a universal occurrence, or is

it specific to particular models? Observing that non-Hermitian Hamiltonians at IPs inherently adopt a Jordan block structure, we employ the perturbation theory of Jordan matrices [57–61] to demonstrate the generality of the phenomenon. At the same time, we establish a universal condition under which a perturbation of strength  $\epsilon$  guarantees the spectral splitting scales as  $\sqrt[k]{\epsilon}$ .

Consider a general 1D non-Hermitian lattice system of length  $L$ , where the Hamiltonian at an IP is denoted by  $H_{\text{IP}}$ . Without loss of generality, assume that  $H_{\text{IP}}$  has a right eigenstate  $|u_0\rangle$  (which is not a topological mode) at an energy  $E = E_{\text{IP}}$ , with its corresponding left eigenstate being  $|v_0\rangle$ . Since the emergence of an IP stems from the collapse of the generalized Brillouin zone [50], all eigenstates of a band will coalesce to one at the IP. Therefore,  $E_{\text{IP}}$  can also be viewed as a nonderogatory eigenenergy [62] of  $H_{\text{IP}}$  [57] whose algebraic multiplicity is  $k = L - \alpha$ . Here  $k$  represents the number of eigenstates within a band, while  $\alpha$  is a finite integer that counts the number of topological modes in the system, which is independent of the system's size  $L$ .

Next consider the presence of a perturbation  $H_{\text{pert}} = \epsilon H_1$  with  $\epsilon \ll 1$  being a dimensionless parameter. The perturbation theory of Jordan matrix [57–61] tells that, if  $\langle v_0 | H_1 | u_0 \rangle = \Lambda$  is nonzero, then the perturbed eigenenergies and eigenstates with the leading-order corrections are given by (a physical approach to the case when  $H_1$  only contains hoppings between the two ends of the system is provided in Sec. II of the SM [55])

$$E_{p,i} = E_{\text{IP}} + \epsilon^{\frac{1}{k}} e_i + o(\epsilon^{\frac{1}{k}}) \quad (i = 1, 2, \dots, k), \quad (6)$$

$$|u_{p,i}\rangle = |u_0\rangle + \epsilon^{\frac{1}{k}} e_i |u_1\rangle + o(\epsilon^{\frac{1}{k}}) \quad (i = 1, 2, \dots, k), \quad (7)$$

where  $e_i$  with  $i = 1, 2, \dots, k$  denotes the  $i$ -th root of the equation  $e - \Lambda^{\frac{1}{k}} = 0$ ;  $|u_{p,i}\rangle$  is the eigenstate associated with the eigenenergy  $E_{p,i}$ , and  $|u_1\rangle$  satisfies  $(H_{\text{IP}} - E_{\text{IP}})|u_1\rangle = |u_0\rangle$ . Eqs. (6) and (7) reveal that if  $\Lambda$  is nonzero, the perturbation  $H_{\text{pert}}$  will split the coalescence and recover the existence of  $k$  eigenstates, and importantly, the splitting of eigenenergies is proportional to  $\sqrt[k]{\epsilon} \sim \sqrt[k]{\epsilon}$  when  $L$  is much larger than  $\alpha$ . Since  $\lim_{L \rightarrow \infty} \sqrt[k]{\epsilon} = 1$  for  $\forall \epsilon > 0$ , a target signal inducing an arbitrarily weak boundary-coupling perturbation to non-Hermitian systems at an IP will become detectable in the limit of sufficiently large system size  $L$ . This sensitivity scaling far exceeds that achievable with conventional EPs [36, 39], suggesting that IPs could enable super-enhanced sensor designs through their unique spectral properties.

In Ref. [50], it has been shown that all right eigenstates at an IP are localized at finite sites near the boundary of the system, and similarly, all corresponding left eigenstates are extremely localized at the opposite boundary. Hence,  $|u_0\rangle$  and  $|v_0\rangle$  are localized at opposite ends (see more discussions in Sec. II of the SM [55]). To make  $\langle v_0 | H_1 | u_0 \rangle$  nonzero, it is evident that a natural and physical choice of the perturbation  $H_1$  is to contain the hopping between the two ends of the system, as previously

illustrated by the HN model. Since all results in this section are independent of the specific form of  $H_{\text{IP}}$ , it suggests that the eigenenergies of any 1D non-Hermitian lattice system at an IP will always be extremely sensitive to hoppings between the two ends of the system. In Sec. III of the SM [55], we demonstrate the model-independence of this phenomenon using a completely different model.

Before concluding this section, we compare our results with the non-Hermitian topological sensor proposed in Ref. [63]. Focusing on topological zero modes, the authors showed via perturbation theory that a boundary-coupling perturbation induces an exponential energy shift of the form:  $\Delta E \approx \epsilon \kappa e^{\alpha L}$  for  $L \gg 1$ , where  $\kappa$  and  $\alpha$  are model-dependent parameters. Although this sensitivity also grows exponentially with system size, the scaling  $\Delta E \sim \epsilon$  (for fixed  $L$ ) contrasts sharply with the  $\sqrt[k]{\epsilon}$  dependence, indicating fundamentally distinct underlying mechanisms. Moreover, the formula  $\Delta E \approx \epsilon \kappa e^{\alpha L}$  is only physically meaningful below a critical system size, as it would otherwise diverge unphysically as  $L \rightarrow +\infty$ . In contrast, these formulas in Eqs. (6) and (7) remain valid for arbitrarily large  $L$ , since  $\lim_{L \rightarrow \infty} \sqrt[k]{\epsilon} = 1$ . The most significant distinction lies in the scope of description: while the formula developed in Ref. [63] specially addressed the behavior of topological zero modes, our framework provides a complete characterization encompassing all eigenstates except the topological modes through Eqs. (6) and (7). This demonstrates that IP-based sensitivity is inherently a collective phenomenon, offering the practical advantage of signal detection without requiring mode-specific measurements—a substantial simplification for potential implementations.

*Robustness of the phenomenon*—While the special property of IPs can result in super-enhanced sensitivity to perturbations fulfilling the condition discussed above, the occurrence of IPs typically hinges on a precise tuning of the system's parameters [50]. If this super-enhanced sensitivity were confined solely to systems exactly at an IP, its practical applications would be severely limited. Therefore, it is crucial to investigate whether this heightened sensitivity persists even when the system deviates from the exact IP. Fortunately, our findings affirm that it does, highlighting the robustness of this phenomenon.

Again we use the HN model to demonstrate the robustness of the phenomenon. Now we set  $t_l = 1$  and  $t_r = \delta \ll 1$ , so that the system deviates from the precise IP at  $t_r = 0$ . According to the non-Bloch band theory [64], the spectrum for a system with length  $L$  subject to OBC is given by  $E(\delta, q) = 2\sqrt{\delta} \cos q$ , where  $q = 0, 2\pi/L, \dots, 2\pi(L-1)/L$ . It is evident that the band width is exclusively determined by  $\delta$  and is independent of  $L$ . The numerical results presented in Fig. 2 show that the eigenenergies remain exceptionally sensitive to the boundary-coupling perturbation given in Eq. (2) even though the system deviates from the precise IP. Particularly, we find that the perturbed eigenenergies are still approximately equal to  $\sqrt[k]{\epsilon}$  even if  $\epsilon \ll \delta$  ( $\epsilon_r = \epsilon_l = \epsilon$  is set), demonstrating the robustness of the phenomenon.

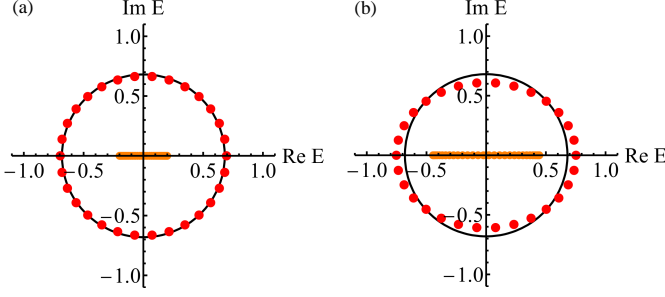


FIG. 2. The spectrum of the HN model away from the IP. The orange dots depict eigenenergies without considering the boundary-coupling perturbation, while the dots in red depict eigenenergies in the presence of the perturbation. We set  $\epsilon_r = \epsilon_l = \epsilon$ , and the radius of the black circle is given by  $\sqrt[4]{\epsilon}$  with  $L = 30$  and  $\epsilon = 10^{-5}$ . In panel (a),  $t_l = 1$ , and  $\delta = 0.01$ . In panel (b),  $t_l = 1$ , and  $\delta = 0.05$ .

To understand the robustness of the phenomenon uncovered above, we employ the perturbation theory again. To be specific, we start with  $H_{\text{IP}}$  and treat the hopping leading to the deviation of the system from the IP as a perturbation,  $H_\delta = \delta H_2$ , where  $\delta \ll 1$  is also a dimensionless parameter and  $H_2$  preserve the translation symmetry within the open-boundary system (the hopping range of the terms in  $H_\delta$  are assumed to be finite). Before adding the perturbation  $H_{\text{pert}}$ , the whole system is described by  $H_{\text{IP}} + H_\delta$ . Based on the non-Bloch band theory [50, 64], the generalized Brillouin zone of this system will be split from a point to a closed curve, and the spectrum satisfies

$$[E(\beta(\delta)) - E_{\text{IP}}] \propto \delta^r, \quad (8)$$

where  $\beta(\delta)$  characterizes the generalized Brillouin zone, and  $r > 0$  is a finite rational number, which is independent of the system size. Take the HN model as an example. If we choose  $H_{\text{IP}} = \sum_n c_{n-1}^\dagger c_n$  and  $H_\delta = \delta \sum_n c_{n+1}^\dagger c_n$ . In this case,  $E_{\text{IP}} = 0$ ,  $E(\beta(\delta)) - E_{\text{IP}} = 2\sqrt{\delta} \cos q \propto \sqrt{\delta}$ , indicating  $r = 1/2$ .

To assess the impact of the perturbation  $H_{\text{pert}}$ , it is important to first recognize that  $H_{\text{pert}}$  should not be considered as a minor disturbance to  $H_{\text{IP}} + H_\delta$ . To illustrate this point, let's once again consider the HN model as an example. For the total Hamiltonian  $H_{\text{IP}} + H_\delta$ , the right eigenstate corresponding to  $E(\beta(\delta))$  is  $|u(\beta(\delta))\rangle = \frac{1}{\sqrt{L}}(1, \beta, \beta^2, \dots, \beta^{L-1})^T$  and its left eigenstate is  $\langle v(\beta(\delta))| = \frac{1}{\sqrt{L}}(1, \beta^{-1}, \beta^{-2}, \dots, \beta^{-(L-1)})$ . The left and right eigenstates satisfy  $\langle v(\beta(\delta))|u(\beta(\delta))\rangle = 1$ . Employing the perturbation theory, the correction to  $E(\beta(\delta))$  induced by  $H_p$  given in Eq. (2) is

$$\begin{aligned} \Delta E(\beta(\delta)) &\approx \langle v(\beta(\delta))|H_p|u(\beta(\delta))\rangle \\ &= \frac{1}{L}(\epsilon_r \beta^{L-1} + \epsilon_l \beta^{-(L-1)}). \end{aligned} \quad (9)$$

Since  $|\beta(\delta)|$  is smaller than 1 for  $\delta < 1$ ,  $\Delta E(\beta(\delta))$  always goes divergent as  $L$  goes to infinity. This result indicates

that the eigenenergies of this system is more sensitive to the hopping between the two ends than other types of perturbations. The divergence of  $\Delta E(\beta(\delta))$  suggests that treating  $H_p$  as a perturbation to  $H_{\text{IP}} + H_\delta$  cannot yield the accurate spectrum. Given that  $H_p$  exerts a greater influence on the spectrum compared to  $H_\delta$ , it is more appropriate to treat  $H_\delta$  as a perturbation to  $H_{\text{IP}} + H_p$ .

Based on the eigenenergies and eigenstates of  $H_{\text{IP}} + H_{\text{pert}}$  given in Eqs. (6) and (7), the eigenenergies, after taking into account the first-order corrections induced by  $H_\delta$ , are modified as  $\tilde{E}_{p,i} \approx E_{p,i} + \langle v_{p,i}|H_\delta|u_{p,i}\rangle$ , where  $|v_{p,i}\rangle$  is the corresponding left eigenstate of  $|u_{p,i}\rangle$  and  $\langle v_{p,i}|u_{p,j}\rangle = \delta_{ij}$  [65]. Write down the result explicitly,

$$\tilde{E}_{p,i} \approx E_{\text{IP}} + \epsilon^{\frac{1}{k}} e_i + \delta \langle v_{p,i}|H_2|u_{p,i}\rangle. \quad (10)$$

When the system's size is sufficiently large, the second term on the right-hand side of Eq. (10) can dominate the third term over a broad range of  $\delta$ . This result suggests that the exceptional sensitivity of eigenenergies to  $H_{\text{pert}}$  can persist even when the system deviates substantially from the IP, as illustrated in Fig. 2(b).

*Discussions and conclusions*—The IP that arises in open-boundary non-Hermitian systems offers a versatile route to achieving EPs of arbitrarily high order through mere adjustment of the system's size. When such a system is at an IP, we have shown that a perturbation of strength  $\epsilon$ , which couples the two opposing boundaries of the system, causes the eigenenergies to split according to the law  $\sqrt[k]{\epsilon}$ , where  $k$  is proportional to the system's length and represents the order of the EP. Utilizing the perturbation theory of Jordan matrices, we have demonstrated that the sensitivity of the eigenenergies to this type of boundary-coupling perturbation is a ubiquitous phenomenon. Moreover, based on both perturbation theory and exact numerical calculations, we have confirmed that this phenomenon remains robust even when the system deviates substantially from the IP.

The observation of the phenomenon predicted in this paper is within the current state-of-the-art experimental conditions. Specifically, the sensitivity of the eigenenergies to boundary-coupling perturbations stems from the significant discrepancy in the spectra of non-Hermitian systems under OBC and PBC. This sensitivity makes it possible to observe a strong response of the eigenenergies to perturbations in systems that exhibit strong non-Hermitian skin effects. Notably, such systems have been implemented across a diverse range of flexible platforms, including metamaterials [66], cold-atom systems [67, 68], electric circuits [69–72], phononic crystals [73], acoustic systems [74, 75] and others [76]. On the basis of these systems implemented in experiments, we anticipate that the super-enhanced sensitivity of the eigenenergies to perturbations will be observed as the system is designed to approach the IP.

In summary, the eigenenergies of non-Hermitian systems at IPs collectively exhibit exceptional sensitivity to boundary-coupling perturbations. This unique property

holds great potential for applications involving sensitive measurements.

*Acknowledgments*—We thank Zheng-Yang Zhuang and Yao Zhou for helpful discussions. This work is sup-

ported by the National Natural Science Foundation of China (Grant No. 12174455) and Guangdong Basic and Applied Basic Research Foundation (Grant No. 2023B1515040023).

- 
- [1] H. J. Carmichael, Quantum trajectory theory for cascaded open systems, *Phys. Rev. Lett.* **70**, 2273 (1993).
  - [2] I. Rotter, A non-hermitian hamilton operator and the physics of open quantum systems, *Journal of Physics A: Mathematical and Theoretical* **42**, 153001 (2009).
  - [3] W. D. Heiss, Exceptional points of non-hermitian operators, *Journal of Physics A: Mathematical and General* **37**, 2455 (2004).
  - [4] M. V. Berry, Physics of nonhermitian degeneracies, *Czechoslovak journal of physics* **54**, 1039 (2004).
  - [5] H. Shen, B. Zhen, and L. Fu, Topological band theory for non-hermitian hamiltonians, *Phys. Rev. Lett.* **120**, 146402 (2018).
  - [6] K. Kawabata, T. Bessho, and M. Sato, Classification of exceptional points and non-hermitian topological semimetals, *Phys. Rev. Lett.* **123**, 066405 (2019).
  - [7] H. Hu, S. Sun, and S. Chen, Knot topology of exceptional point and non-hermitian no-go theorem, *Phys. Rev. Res.* **4**, L022064 (2022).
  - [8] Z. Yang, C.-K. Chiu, C. Fang, and J. Hu, Jones polynomial and knot transitions in hermitian and non-hermitian topological semimetals, *Phys. Rev. Lett.* **124**, 186402 (2020).
  - [9] Z. Yang, A. P. Schnyder, J. Hu, and C.-K. Chiu, Fermion doubling theorems in two-dimensional non-hermitian systems for fermi points and exceptional points, *Phys. Rev. Lett.* **126**, 086401 (2021).
  - [10] T. Liu, J. J. He, Z. Yang, and F. Nori, Higher-order weyl-exceptional-ring semimetals, *Phys. Rev. Lett.* **127**, 196801 (2021).
  - [11] S. Jana and L. Sirota, Emerging exceptional point with breakdown of the skin effect in non-hermitian systems, *Phys. Rev. B* **108**, 085104 (2023).
  - [12] J. L. K. König, K. Yang, J. C. Budich, and E. J. Bergholtz, Braid-protected topological band structures with unpaired exceptional points, *Phys. Rev. Res.* **5**, L042010 (2023).
  - [13] Y. Xu, S.-T. Wang, and L.-M. Duan, Weyl exceptional rings in a three-dimensional dissipative cold atomic gas, *Phys. Rev. Lett.* **118**, 045701 (2017).
  - [14] Z. Yang and J. Hu, Non-hermitian hopf-link exceptional line semimetals, *Phys. Rev. B* **99**, 081102 (2019).
  - [15] J. Carlström, M. Stålhammar, J. C. Budich, and E. J. Bergholtz, Knotted non-hermitian metals, *Phys. Rev. B* **99**, 161115 (2019).
  - [16] A. Cerjan, M. Xiao, L. Yuan, and S. Fan, Effects of non-hermitian perturbations on weyl hamiltonians with arbitrary topological charges, *Phys. Rev. B* **97**, 075128 (2018).
  - [17] R. Okugawa and T. Yokoyama, Topological exceptional surfaces in non-hermitian systems with parity-time and parity-particle-hole symmetries, *Phys. Rev. B* **99**, 041202 (2019).
  - [18] W. B. Rui, Z. Zheng, C. Wang, and Z. D. Wang, Non-hermitian spatial symmetries and their stabilized normal and exceptional topological semimetals, *Phys. Rev. Lett.* **128**, 226401 (2022).
  - [19] P. Delplace, T. Yoshida, and Y. Hatsugai, Symmetry-protected multifold exceptional points and their topological characterization, *Phys. Rev. Lett.* **127**, 186602 (2021).
  - [20] J. T. Gohsrich, J. Fauman, and F. K. Kunst, Exceptional points of any order in a generalized hatano-nelson model (2024), arXiv:2403.12018 [cond-mat.mes-hall].
  - [21] Z.-J. Li, G. Cardoso, E. J. Bergholtz, and Q.-D. Jiang, Braids and higher-order exceptional points from the interplay between lossy defects and topological boundary states, *Phys. Rev. Res.* **6**, 043023 (2024).
  - [22] K. Ding, G. Ma, M. Xiao, Z. Q. Zhang, and C. T. Chan, Emergence, coalescence, and topological properties of multiple exceptional points and their experimental realization, *Phys. Rev. X* **6**, 021007 (2016).
  - [23] H. Zhou, J. Y. Lee, S. Liu, and B. Zhen, Exceptional surfaces in pt-symmetric non-hermitian photonic systems, *Optica* **6**, 190 (2019).
  - [24] C. Dembowski, H.-D. Gräf, H. L. Harney, A. Heine, W. D. Heiss, H. Rehfeld, and A. Richter, Experimental observation of the topological structure of exceptional points, *Phys. Rev. Lett.* **86**, 787 (2001).
  - [25] S. Klaiman, U. Günther, and N. Moiseyev, Visualization of branch points in  $\mathcal{PT}$ -symmetric waveguides, *Phys. Rev. Lett.* **101**, 080402 (2008).
  - [26] S.-B. Lee, J. Yang, S. Moon, S.-Y. Lee, J.-B. Shim, S. W. Kim, J.-H. Lee, and K. An, Observation of an exceptional point in a chaotic optical microcavity, *Phys. Rev. Lett.* **103**, 134101 (2009).
  - [27] J. Zhu, Şahin Kaya Özdemir, L. He, and L. Yang, Controlled manipulation of mode splitting in an optical microcavity by two rayleigh scatterers, *Opt. Express* **18**, 23535 (2010).
  - [28] B. Peng, Şahin Kaya Özdemir, M. Liertzer, W. Chen, J. Kramer, H. Yılmaz, J. Wiersig, S. Rotter, and L. Yang, Chiral modes and directional lasing at exceptional points, *Proceedings of the National Academy of Sciences* **113**, 6845 (2016).
  - [29] A. Regensburger, C. Bersch, M.-A. Miri, G. Onishchukov, D. N. Christodoulides, and U. Peschel, Parity-time synthetic photonic lattices, *Nature* **488**, 167 (2012).
  - [30] B. Zhen, C. W. Hsu, Y. Igarashi, L. Lu, I. Kaminer, A. Pick, S.-L. Chua, J. D. Joannopoulos, and M. Soljačić, Spawning rings of exceptional points out of dirac cones, *Nature* **525**, 354 (2015).
  - [31] H. Zhou, C. Peng, Y. Yoon, C. W. Hsu, K. A. Nelson, L. Fu, J. D. Joannopoulos, M. Soljačić, and B. Zhen, Observation of bulk fermi arc and polarization half charge from paired exceptional points, *Science* **359**, 1009 (2018).
  - [32] A. Cerjan, S. Huang, M. Wang, K. P. Chen, Y. Chong, and M. C. Rechtsman, Experimental realization of a weyl exceptional ring, *Nature Photonics* **13**, 623 (2019).
  - [33] W. Tang, X. Jiang, K. Ding, Y.-X. Xiao, Z.-Q. Zhang,

- C. T. Chan, and G. Ma, Exceptional nexus with a hybrid topological invariant, *Science* **370**, 1077 (2020).
- [34] X. Zhang, K. Ding, X. Zhou, J. Xu, and D. Jin, Experimental observation of an exceptional surface in synthetic dimensions with magnon polaritons, *Phys. Rev. Lett.* **123**, 237202 (2019).
- [35] Y. Choi, S. Kang, S. Lim, W. Kim, J.-R. Kim, J.-H. Lee, and K. An, Quasieigenstate coalescence in an atom-cavity quantum composite, *Phys. Rev. Lett.* **104**, 153601 (2010).
- [36] J. Wiersig, Enhancing the sensitivity of frequency and energy splitting detection by using exceptional points: Application to microcavity sensors for single-particle detection, *Phys. Rev. Lett.* **112**, 203901 (2014).
- [37] J. Wiersig, Sensors operating at exceptional points: General theory, *Phys. Rev. A* **93**, 033809 (2016).
- [38] W. Chen, Ş. Kaya Özdemir, G. Zhao, J. Wiersig, and L. Yang, Exceptional points enhance sensing in an optical microcavity, *Nature* **548**, 192 (2017).
- [39] H. Hodaei, A. U. Hassan, S. Wittek, H. Garcia-Gracia, R. El-Ganainy, D. N. Christodoulides, and M. Khajavikhan, Enhanced sensitivity at higher-order exceptional points, *Nature* **548**, 187 (2017).
- [40] W. Langbein, No exceptional precision of exceptional-point sensors, *Phys. Rev. A* **98**, 023805 (2018).
- [41] Z. Xiao, H. Li, T. Kottos, and A. Alù, Enhanced sensing and nondegraded thermal noise performance based on  $\mathcal{PT}$ -symmetric electronic circuits with a sixth-order exceptional point, *Phys. Rev. Lett.* **123**, 213901 (2019).
- [42] Q. Zhong, J. Ren, M. Khajavikhan, D. N. Christodoulides, S. K. Özdemir, and R. El-Ganainy, Sensing with exceptional surfaces in order to combine sensitivity with robustness, *Phys. Rev. Lett.* **122**, 153902 (2019).
- [43] P. Djourwe, Y. Pennec, and B. Djafari-Rouhani, Exceptional point enhances sensitivity of optomechanical mass sensors, *Phys. Rev. Appl.* **12**, 024002 (2019).
- [44] S. Yu, Y. Meng, J.-S. Tang, X.-Y. Xu, Y.-T. Wang, P. Yin, Z.-J. Ke, W. Liu, Z.-P. Li, Y.-Z. Yang, G. Chen, Y.-J. Han, C.-F. Li, and G.-C. Guo, Experimental investigation of quantum  $\mathcal{PT}$ -enhanced sensor, *Phys. Rev. Lett.* **125**, 240506 (2020).
- [45] J. Wiersig, Robustness of exceptional-point-based sensors against parametric noise: The role of hamiltonian and liouvillian degeneracies, *Phys. Rev. A* **101**, 053846 (2020).
- [46] P. Djourwé, M. Asjad, Y. Pennec, D. Dutykh, and B. Djafari-Rouhani, Parametrically enhancing sensor sensitivity at an exceptional point, *Phys. Rev. Res.* **6**, 033284 (2024).
- [47] M. M. Denner, A. Skurativska, F. Schindler, M. H. Fischer, R. Thomale, T. Bzdušek, and T. Neupert, Exceptional topological insulators, *Nature communications* **12**, 5681 (2021).
- [48] M. M. Denner, T. Neupert, and F. Schindler, Infernal and exceptional edge modes: non-hermitian topology beyond the skin effect, *Journal of Physics: Materials* **6**, 045006 (2023).
- [49] Y. Fu and S. Wan, Degeneracy and defectiveness in non-hermitian systems with open boundary, *Phys. Rev. B* **105**, 075420 (2022).
- [50] S.-X. Wang and Z. Yan, General theory for infernal points in non-hermitian systems, *Phys. Rev. B* **110**, L201104 (2024).
- [51] I. Mandal and E. J. Bergholtz, Symmetry and Higher-Order Exceptional Points, *Phys. Rev. Lett.* **127**, 186601 (2021).
- [52] S. M. Zhang, X. Z. Zhang, L. Jin, and Z. Song, High-order exceptional points in supersymmetric arrays, *Phys. Rev. A* **101**, 033820 (2020).
- [53] N. Hatano and D. R. Nelson, Localization transitions in non-hermitian quantum mechanics, *Phys. Rev. Lett.* **77**, 570 (1996).
- [54] S. Yao and Z. Wang, Edge states and topological invariants of non-hermitian systems, *Phys. Rev. Lett.* **121**, 086803 (2018).
- [55] The supplemental material contains the details of: (I) Derivation for Eq.(4). (II) A physical approach for Eqs. (6) and (7). (III) Generalized non-Hermitian SSH model as a further example.
- [56] C.-X. Guo, L. Su, Y. Wang, L. Li, J. Wang, X. Ruan, Y. Du, D. Zheng, S. Chen, and H. Hu, Scale-tailored localization and its observation in non-hermitian electrical circuits, *Nature Communications* **15**, 9120 (2024).
- [57] A. P. Seyranian and A. A. Mailybaev, *Multiparameter stability theory with mechanical applications*, Vol. 13 (World Scientific, 2003).
- [58] V. B. Lidskii, Perturbation theory of non-conjugate operators, *USSR Computational Mathematics and Mathematical Physics* **6**, 73 (1966).
- [59] Y. Ma and A. Edelman, Nongeneric eigenvalue perturbations of jordan blocks, *Linear Algebra and its Applications* **273**, 45 (1998).
- [60] M. I. Vishik and L. A. Lyusternik, The solution of some perturbation problems for matrices and selfadjoint or non-selfadjoint differential equations i, *Russian Mathematical Surveys* **15**, 1 (1960).
- [61] J. Moro, J. V. Burke, and M. L. Overton, On the lidskii-vishik-lyusternik perturbation theory for eigenvalues of matrices with arbitrary jordan structure, *SIAM Journal on Matrix Analysis and Applications* **18**, 793 (1997).
- [62] Nonderogatory eigenenergy here means that the geometric multiplicity of this eigenenergy is one.
- [63] J. C. Budich and E. J. Bergholtz, Non-hermitian topological sensors, *Phys. Rev. Lett.* **125**, 180403 (2020).
- [64] K. Yokomizo and S. Murakami, Non-bloch band theory of non-hermitian systems, *Phys. Rev. Lett.* **123**, 066404 (2019).
- [65] After including the perturbation  $H_{\text{pert}}$ , the eigenenergy splits, and  $E_{p,i}$  is no longer a nonderogatory eigenenergy but becomes a simple eigenenergy. Thus  $|v_{p,i}\rangle \neq |v_0\rangle + \epsilon^{\frac{1}{k}} e_i^* |v_1\rangle + o(\epsilon^{\frac{1}{k}})$ .
- [66] X. Zhang, Y. Tian, J.-H. Jiang, M.-H. Lu, and Y.-F. Chen, Observation of higher-order non-hermitian skin effect, *Nature Communications* **12**, 5377 (2021).
- [67] Q. Liang, D. Xie, Z. Dong, H. Li, H. Li, B. Gadway, W. Yi, and B. Yan, Dynamic signatures of non-hermitian skin effect and topology in ultracold atoms, *Phys. Rev. Lett.* **129**, 070401 (2022).
- [68] E. Zhao, Z. Wang, C. He, T. F. J. Poon, K. K. Pak, Y.-J. Liu, P. Ren, X.-J. Liu, and G.-B. Jo, Two-dimensional non-hermitian skin effect in an ultracold fermi gas, *Nature*, 1 (2025).
- [69] T. Hofmann, T. Helbig, F. Schindler, N. Salgo, M. Brzezińska, M. Greiter, T. Kiessling, D. Wolf, A. Vollhardt, A. Kabaši, C. H. Lee, A. Bilušić, R. Thomale, and

- T. Neupert, Reciprocal skin effect and its realization in a topoelectrical circuit, *Phys. Rev. Res.* **2**, 023265 (2020).
- [70] W. Zhang, F. Di, H. Yuan, H. Wang, X. Zheng, L. He, H. Sun, and X. Zhang, Observation of non-hermitian aggregation effects induced by strong interactions, *Phys. Rev. B* **105**, 195131 (2022).
  - [71] D. Zou, T. Chen, W. He, J. Bao, C. H. Lee, H. Sun, and X. Zhang, Observation of hybrid higher-order skin-topological effect in non-hermitian topoelectrical circuits, *Nature Communications* **12**, 7201 (2021).
  - [72] V. Könye, K. Ochkan, A. Chyzykova, J. C. Budich, J. van den Brink, I. C. Fulga, and J. Dufouleur, Non-hermitian topological ohmmeter, *Phys. Rev. Appl.* **22**, L031001 (2024).
  - [73] Q. Zhou, J. Wu, Z. Pu, J. Lu, X. Huang, W. Deng, M. Ke, and Z. Liu, Observation of geometry-dependent skin effect in non-hermitian phononic crystals with exceptional points, *Nature Communications* **14**, 4569 (2023).
  - [74] L. Zhang, Y. Yang, Y. Ge, Y.-J. Guan, Q. Chen, Q. Yan, F. Chen, R. Xi, Y. Li, D. Jia, *et al.*, Acoustic non-hermitian skin effect from twisted winding topology, *Nature communications* **12**, 6297 (2021).
  - [75] Q. Zhang, Y. Li, H. Sun, X. Liu, L. Zhao, X. Feng, X. Fan, and C. Qiu, Observation of acoustic non-hermitian bloch braids and associated topological phase transitions, *Phys. Rev. Lett.* **130**, 017201 (2023).
  - [76] W. Wang, M. Hu, X. Wang, G. Ma, and K. Ding, Experimental realization of geometry-dependent skin effect in a reciprocal two-dimensional lattice, *Phys. Rev. Lett.* **131**, 207201 (2023).

# Supplemental Material for “Super-enhanced Sensitivity in Non-Hermitian Systems at Infernal Points”

## I. DETAILED DERIVATION OF EQ. (4)

For the Hamiltonian given in Eq.(3), its characteristic polynomial is determined by calculating the determinant of the following matrix,

$$H - \lambda \mathbb{I}_{L \times L} = \begin{pmatrix} -\lambda & t_l & & \epsilon_r \\ 0 & -\lambda & t_l & \\ & \ddots & \ddots & \ddots \\ & & 0 & -\lambda & t_l \\ \epsilon_l & & & 0 & -\lambda \end{pmatrix}_{L \times L}. \quad (\text{S1})$$

By expanding the determinant according to the first column,

$$\begin{aligned} f(\lambda) &= \det [H - \lambda \mathbb{I}_{L \times L}] \\ &= -\lambda \det \left[ \begin{pmatrix} -\lambda & t_l & & \\ 0 & -\lambda & t_l & \\ & \ddots & \ddots & \ddots \\ & & 0 & -\lambda & t_l \\ & & & 0 & -\lambda \end{pmatrix}_{(L-1) \times (L-1)} \right] \\ &\quad + (-1)^{L-1} \epsilon_l \det \left[ \begin{pmatrix} t_l & 0 & & \epsilon_r \\ -\lambda & t_l & 0 & \\ & \ddots & \ddots & \ddots \\ & & \ddots & \ddots & 0 \\ & & & -\lambda & t_l \end{pmatrix}_{(L-1) \times (L-1)} \right] \\ &= -\lambda f_1 + (-1)^{L-1} \epsilon_l f_2. \end{aligned} \quad (\text{S2})$$

Apparently,  $f_1 = (-\lambda)^{L-1}$  and

$$\begin{aligned} f_2 &= t_l \det \left[ \begin{pmatrix} t_l & & & \\ -\lambda & t_l & & \\ & \ddots & \ddots & \\ & & -\lambda & t_l \end{pmatrix}_{(L-2) \times (L-2)} \right] \\ &\quad + (-1)^{L-2} \epsilon_r \det \left[ \begin{pmatrix} -\lambda & t_l & & \\ & \ddots & \ddots & \\ & & \ddots & t_l \\ & & & -\lambda \end{pmatrix}_{(L-2) \times (L-2)} \right] \\ &= t_l^{L-1} + (-1)^{L-2} (-\lambda)^{L-2} \epsilon_r. \end{aligned} \quad (\text{S3})$$

Therefore, one finds

$$\begin{aligned} f(\lambda) &= (-\lambda)^L + (-1)^{L-1} \epsilon_l [t_l^{L-1} + (-1)^{L-2} (-\lambda)^{L-2} \epsilon_r] \\ &= (-\lambda)^L + (-1)^{L-1} \epsilon_l t_l^{L-1} - \epsilon_l \epsilon_r (-\lambda)^{L-2}, \end{aligned} \quad (\text{S4})$$

which is the result presented in Eq. (4) of the main text.

## II. A PHYSICAL APPROACH TO OBTAIN EQS. (6) AND (7)

In this section, we provide a simplified proof of Eqs. (6) and (7) in the main text for the case that  $H_1$  only contains hoppings between the two ends of the system.



When the system resides at an IP, the eigenenergy  $E_{\text{IP}}$  can be viewed as a nonderogatory eigenvalue of the Hamiltonian  $H_{\text{IP}}$  with multiplicity  $k$ . Thus, the Hilbert space corresponding to  $E_{\text{IP}}$  is composed of the eigenvector  $|u_0\rangle$  and  $k-1$  associated vectors  $|u_1\rangle, |u_2\rangle, \dots, |u_{k-1}\rangle$ , which compose a Jordan chain, i.e.,

$$\begin{aligned} (H_{\text{IP}} - E_{\text{IP}})|u_0\rangle &= 0, \\ (H_{\text{IP}} - E_{\text{IP}})|u_1\rangle &= |u_0\rangle, \\ &\vdots \\ (H_{\text{IP}} - E_{\text{IP}})|u_{k-1}\rangle &= |u_{k-2}\rangle. \end{aligned} \tag{S5}$$

Similarly, the left eigenvector  $\langle v_0|$  corresponding to  $E_{\text{IP}}$  and the  $k-1$  associated vectors  $\langle v_1|, \langle v_2|, \dots, \langle v_{k-1}|$  compose the left Jordan chain, i.e,

$$\begin{aligned} \langle v_0| (H_{\text{IP}} - E_{\text{IP}}) &= 0, \\ \langle v_1| (H_{\text{IP}} - E_{\text{IP}}) &= \langle v_0|, \\ &\vdots \\ \langle v_{k-1}| (H_{\text{IP}} - E_{\text{IP}}) &= \langle v_{k-2}|. \end{aligned} \tag{S6}$$

The left and right eigenvectors satisfy the orthogonal normalization condition[57]

$$\langle v_i|u_j\rangle = \delta_{i+j,k-1} \quad (i, j = 0, 1, \dots, k-1). \tag{S7}$$

It is worth noting that this orthogonal normalization condition differs somewhat from the typical biorthogonal normalization condition used to describe non-Hermitian Hamiltonians whose eigenstates are devoid of defectiveness.

Now, we add the perturbation  $H_{\text{pert}} = \epsilon H_1$  and assume that the original eigenenergy  $E_{\text{IP}}$  is modified as  $E_{\text{IP}} + \lambda_1$ , and the eigenstate  $|u_0\rangle$  is modified as

$$|u\rangle = |u_0\rangle + \sum_{i=1}^{k-1} s_i |u_i\rangle, \tag{S8}$$

where  $s_i$  denotes coefficients. Accordingly, the Schrödinger equation for the perturbed system is

$$[H_{\text{IP}} + H_{\text{pert}} - E_{\text{IP}} - \lambda_1] |u\rangle = 0. \tag{S9}$$

Substituting Eqs.(S5) and (S8) into Eq.(S9), we get

$$\sum_{i=1}^{k-1} s_i |u_{i-1}\rangle + (\epsilon H_1 - \lambda_1) \left[ |u_0\rangle + \sum_{i=1}^{k-1} s_i |u_i\rangle \right] = 0. \tag{S10}$$

According to Ref. [50],  $|u_0\rangle$  is extremely localized at one side of the system. Considering the normalization condition given in Eq. (S7), it is straightforward to deduce that  $|u_0\rangle$  and  $|v_{k-1}\rangle$  are both extremely localized on the same side of the system, while  $|u_{k-1}\rangle$  and  $|v_0\rangle$  are localized on the opposite side. Since  $H_1$  only contains hoppings between the two ends of the system, we assume that only two elements of  $\langle v_i|H_1|u_j\rangle$  are nonzero, which are

$$\langle v_0|H_1|u_0\rangle = \Lambda, \quad \langle v_{k-1}|H_1|u_{k-1}\rangle = \Delta. \tag{S11}$$

Using  $\langle v_0|, \langle v_1|, \dots, \langle v_{k-1}|$  to multiply Eq. (S9) from the left side respectively and utilizing Eq.(S7), we obtain

$$\begin{aligned} \epsilon \Lambda - \lambda_1 s_{k-1} &= 0, \\ s_{k-1} - \lambda_1 s_{k-2} &= 0, \\ &\vdots \\ s_2 - \lambda_1 s_1 &= 0, \\ s_1 + \epsilon s_{k-1} \Delta - \lambda_1 &= 0. \end{aligned} \tag{S12}$$

Reducing Eq. (S12), we get

$$s_i = \lambda_1^{i-1} s_1, \tag{S13}$$

$$\epsilon \Lambda - \lambda_1^{k-1} s_1 = 0, \tag{S14}$$

$$\frac{1}{\lambda_1^{k-1}} [\epsilon \Lambda + \epsilon^2 \Lambda \Delta \lambda_1^{k-2} - \lambda_1^k] = 0. \tag{S15}$$

Since  $\epsilon \ll 1$ , we neglect the  $\epsilon^2$  term in Eq. (S15). Under this approximation,  $\lambda_1$  can be solved as

$$\lambda_{1,j} \approx \epsilon^{\frac{1}{k}} e_j \quad (j = 1, 2, \dots, k), \quad (\text{S16})$$

where  $e_j$  for  $j = 1, 2, \dots, k$  denotes the  $j$ -th root of the equation  $e - \Lambda^{\frac{1}{k}} = 0$ . Substituting Eq. (S16) into Eqs. (S13) and (S14), we get

$$s_{i,j} = \left[ \epsilon^{\frac{1}{k}} e_j \right]^i. \quad (\text{S17})$$

This means that the single eigenenergy at the IP is split to  $k$  eigenenergies, whose expressions are

$$E_{p,j} = E_{\text{IP}} + \lambda_{i,j} + o(\epsilon^{\frac{1}{k}}) = E_{\text{IP}} + \epsilon^{\frac{1}{k}} e_j + o(\epsilon^{\frac{1}{k}}) \quad (j = 1, 2, \dots, k), \quad (\text{S18})$$

and the corresponding eigenstates are

$$|u_{p,j}\rangle = |u_0\rangle + \sum_{i=1}^{k-1} s_{i,j} |u_i\rangle \approx |u_0\rangle + \epsilon^{\frac{1}{k}} e_j |u_1\rangle \quad (j = 1, 2, \dots, k). \quad (\text{S19})$$

Eq. (S18) and Eq. (S19) correspond to Eq. (6) and Eq. (7) in the main text, respectively.

### III. GENERALIZED NON-HERMITIAN SSH MODEL AS A FURTHER EXAMPLE

In this section, we employ the generalized non-Hermitian Su-Schrieffer-Heeger (SSH) model as a further example to illustrate that the properties of the IP, as presented in the main text, exhibit universality and are independent of the specific Hamiltonian's form.

The generalized non-Hermitian SSH model is given by [50]

$$\begin{aligned} H_{GSSH} = & \sum_{n=1}^L (t_1 + \gamma) c_{n,A}^\dagger c_{n,B} + (t_1 - \gamma) c_{n,B}^\dagger c_{n,A} \\ & + (t_2 + l) c_{n+1,A}^\dagger c_{n,B} + (t_2 - l) c_{n-1,B}^\dagger c_{n,A} \\ & + (t_3 + \eta) c_{n-1,A}^\dagger c_{n,B} + (t_3 - \eta) c_{n+1,B}^\dagger c_{n,A}, \end{aligned} \quad (\text{S20})$$

where  $A$  and  $B$  denote the sublattice indices, and  $n \in [1, L]$  labels the position of unit cells. According to Ref. [50], this model gives rise to an IP when  $t_2 = -l$  and  $t_3 = \eta$ . At this IP, the system has only two eigenstates,

$$|u_0^{(1)}\rangle = \left( \frac{\sqrt{t_1^2 - \gamma^2}}{t_1 - \gamma}, 1, 0, \dots, 0 \right)^T, \quad (\text{S21})$$

$$|u_0^{(2)}\rangle = \left( -\frac{\sqrt{t_1^2 - \gamma^2}}{t_1 - \gamma}, 1, 0, \dots, 0 \right)^T, \quad (\text{S22})$$

with corresponding eigenenergies equal to  $E^{(1)} = \sqrt{t_1^2 - \gamma^2}$  and  $E^{(2)} = -\sqrt{t_1^2 - \gamma^2}$ , respectively. Both states exhibit  $L$ -fold coalescence. For the convenience of normalization, we set

$$t_3 = \eta = \frac{\sqrt{t_1^2 - \gamma^2}}{2(t_1 - \gamma)}, \quad t_2 = -l = \frac{t_1 - \gamma}{2\sqrt{t_1^2 - \gamma^2}}. \quad (\text{S23})$$

For this case, the  $(L-1)$ -th associated eigenvectors of  $|u_0^{(1)}\rangle$  and  $|u_0^{(2)}\rangle$  are

$$|u_{L-1}^{(1)}\rangle = \left( 0, 0, \dots, 0, \frac{\sqrt{t_1^2 - \gamma^2}}{t_1 - \gamma}, 1 \right)^T, \quad (\text{S24})$$

$$|u_{L-1}^{(2)}\rangle = (-1)^{L-1} \left( 0, 0, \dots, 0, -\frac{\sqrt{t_1^2 - \gamma^2}}{t_1 - \gamma}, 1 \right)^T, \quad (\text{S25})$$

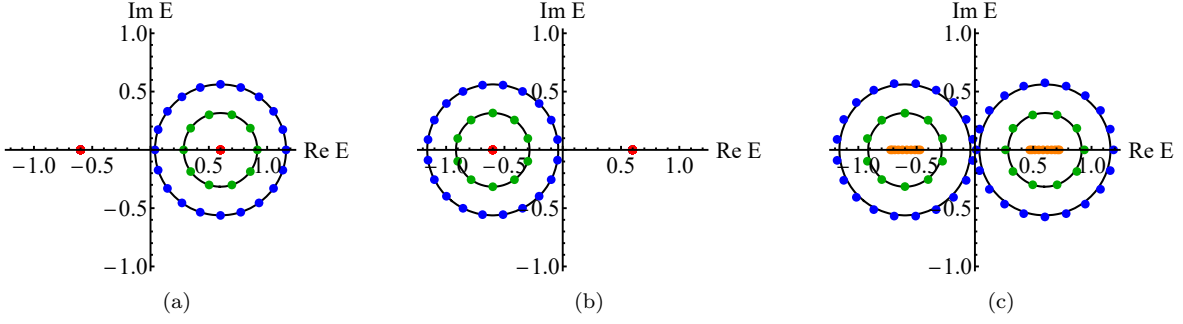


FIG. 3. Spectrum for the generalized non-Hermitian SSH model under open boundary conditions. The red points in (a) and (b) are eigenenergies of the system at the IP when  $t_2 = -l$  and  $t_3 = \eta$ . The two red points correspond to  $E^{(1)} = \sqrt{t_1^2 - \gamma^2}$  and  $E^{(2)} = -\sqrt{t_1^2 - \gamma^2}$ . The orange points in (c) show eigenenergies of the system deviated from the IP with  $t_2 = -l + \delta$ . The green and blue dots refer to spectrum of perturbed system with  $L = 10$  and  $L = 20$ , respectively. (a) Spectrum for the system at the IP under the perturbation  $H_{pert}^{(1)}$  with  $\epsilon_1 = 10^{-5}$ . The radii for the two circles centered at  $E^{(1)}$  are equal to  $\sqrt[10]{\epsilon_1}$  (inner) and  $\sqrt[20]{\epsilon_1}$  (outer). (b) Spectrum under the perturbation  $H_{pert}^{(2)}$  with  $\epsilon_2 = 10^{-5}$ . The radii of the two circles centered at  $E^{(2)}$  are equal to  $\sqrt[10]{\epsilon_2}$  (inner) and  $\sqrt[20]{\epsilon_2}$  (outer). (c) Spectrum under the combined perturbation  $H_{pert}^{(1)} + H_{pert}^{(2)}$  with  $\epsilon_1 = \epsilon_2 = \epsilon = 10^{-5}$ . Right circles (centered at  $E^{(1)}$ ) and left circles (centered at  $E^{(2)}$ ) have radii of the value  $\sqrt[10]{\epsilon}$  (inner) and  $\sqrt[20]{\epsilon}$  (outer). Values of other parameters are  $t_1 = 1$ ,  $\gamma = \frac{4}{5}$ ,  $t_3 = \eta = \frac{3}{2}$ ,  $l = -\frac{1}{6}$  and  $\delta = \frac{1}{40}$ .

respectively. Utilizing the orthogonal normalization condition in Eq. (S7), the corresponding left eigenstates for  $|u_0^{(1)}\rangle$  and  $|u_0^{(2)}\rangle$  can straightforwardly be obtained, which are

$$|v_0^{(1)}\rangle = \frac{1}{2} \left( 0, 0, \dots, 0, \frac{t_1 - \gamma}{\sqrt{t_1^2 - \gamma^2}}, 1 \right)^T, \quad (\text{S26})$$

$$|v_0^{(2)}\rangle = \frac{(-1)^{L-1}}{2} \left( 0, 0, \dots, 0, -\frac{t_1 - \gamma}{\sqrt{t_1^2 - \gamma^2}}, 1 \right)^T, \quad (\text{S27})$$

respectively.

We now consider two independent perturbations that connect opposite ends of the system,

$$H_{pert}^{(1)} = \frac{\epsilon_1}{2} \left( c_{L,A}^\dagger c_{1,A} + c_{L,B}^\dagger c_{1,B} + \frac{\sqrt{t_1^2 - \gamma^2}}{t_1 - \gamma} c_{L,A}^\dagger c_{1,B} + \frac{t_1 - \gamma}{\sqrt{t_1^2 - \gamma^2}} c_{L,B}^\dagger c_{1,A} + h.c. \right), \quad (\text{S28})$$

$$H_{pert}^{(2)} = \frac{\epsilon_2}{2} \left( c_{L,A}^\dagger c_{1,A} + c_{L,B}^\dagger c_{1,B} - \frac{\sqrt{t_1^2 - \gamma^2}}{t_1 - \gamma} c_{L,A}^\dagger c_{1,B} - \frac{t_1 - \gamma}{\sqrt{t_1^2 - \gamma^2}} c_{L,B}^\dagger c_{1,A} + h.c. \right), \quad (\text{S29})$$

where  $\epsilon_1, \epsilon_2 \geq 0$  represent the perturbation strengths. These perturbations satisfy  $|\langle v_0^{(1)} | H_{pert}^{(1)} | u_0^{(1)} \rangle| = \epsilon_1$ ,  $|\langle v_0^{(2)} | H_{pert}^{(2)} | u_0^{(2)} \rangle| = \epsilon_2$ , and  $\langle v_0^{(2)} | H_{pert}^{(1)} | u_0^{(1)} \rangle = \langle v_0^{(1)} | H_{pert}^{(1)} | u_0^{(2)} \rangle = \langle v_0^{(2)} | H_{pert}^{(2)} | u_0^{(1)} \rangle = \langle v_0^{(1)} | H_{pert}^{(2)} | u_0^{(2)} \rangle = 0$ . According to our theory,  $H_{pert}^{(1)}$  will lead to the splitting of  $E^{(1)}$  that scales as  $\sqrt[10]{\epsilon_1}$ , while  $H_{pert}^{(2)}$  similarly affects  $E^{(2)}$  with a scaling of  $\sqrt[10]{\epsilon_2}$ . These predictions are in excellent agreement with the numerical results presented in Fig. S3(a) and Fig. S3(b).

To demonstrate the robustness of the system's extremely high-order sensitivity to perturbations near—but not exactly at—the IP, we set  $t_2 = -l + \delta = \frac{t_1 - \gamma}{2\sqrt{t_1^2 - \gamma^2}} + \delta$ , where  $\delta$  quantifies the departure from the exact IP. To further simplify the picture, we set  $\epsilon_1 = \epsilon_2 = \epsilon$ , so that there is only one parameter to characterize the perturbation strength. As shown in Fig. S3(c), the perturbed spectrum obtained by including  $H_{pert}^{(1)} + H_{pert}^{(2)}$  agrees excellently with the predictions from the Eq. (10) of the main text. This not only confirms the robustness of the system's extremely high-order sensitivity to perturbations even under slight deviations from the IP but also establishes that our theoretical framework for the IP's sensitivity is model-independent.